processes

MDPI

Article

Hierarchical Nanoflowers of Colloidal WS_2 and Their Potential Gas Sensing Properties for Room Temperature Detection of Ammonia

Siziwe S. Gqoba [1,*], Rafael Rodrigues [2], Sharon Lerato Mphahlele [1], Zakhele Ndala [1], Mildred Airo [1], Paul Olawale Fadojutimi [1], Ivo A. Hümmelgen [2], Ella C. Linganiso [1,3], Makwena J. Moloto [4] and Nosipho Moloto [2,*]

1 Molecular Sciences Institute, School of Chemistry, University of The Witwatersrand, Johannesburg 2050, South Africa; leratosharonm@gmail.com (S.L.M.); 491384@students.wits.ac.za (Z.N.); mildred.airo@wits.ac.za (M.A.); 2165101@students.wits.ac.za (P.O.F.); cebisa.linganiso@wits.ac.za (E.C.L.)
2 Departamento de Física, Universidade Federal do Paraná, Curitiba 81531-980, Brazil; rafael779@gmail.com (R.R.); iah@fisica.ufpr.br (I.A.H.)
3 Microscopy and Microanalysis Unit, University of The Witwatersrand, Johannesburg 2050, South Africa
4 Institute for Water Technology and Sustainability, College of Science, Engineering and Technology, University of South Africa, Florida Campus, Johannesburg 1710, South Africa; molotomj@unisa.ac.za
* Correspondence: siziwe.gqoba@wits.ac.za (S.S.G.); nosipho.moloto@wits.ac.za (N.M.); Tel.: +27-11-717-6756 (S.S.G.); +27-11-717-6774 (N.M.)

check for updates

Citation: Gqoba, S.S.; Rodrigues, R.; Mphahlele, S.L.; Ndala, Z.; Airo, M.; Fadojutimi, P.O.; Hümmelgen, I.A.; Linganiso, E.C.; Moloto, M.J.; Moloto, N. Hierarchical Nanoflowers of Colloidal WS_2 and Their Potential Gas Sensing Properties for Room Temperature Detection of Ammonia. *Processes* **2021**, *9*, 1491. https://doi.org/10.3390/pr9091491

Academic Editors: Gugu Hlengiwe Mhlongo and Dimitra Papadaki

Received: 30 June 2021
Accepted: 2 August 2021
Published: 25 August 2021

Abstract: A one-step colloidal synthesis of hierarchical nanoflowers of WS_2 is reported. The nanoflowers were used to fabricate a chemical sensor for the detection of ammonia vapors at room temperature. The gas sensing performance of the WS_2 nanoflowers was measured using an in-house custom-made gas chamber. SEM analysis revealed that the nanoflowers were made up of petals and that the nanoflowers self-assembled to form hierarchical structures. Meanwhile, TEM showed the exposed edges of the petals that make up the nanoflower. A band gap of 1.98 eV confirmed a transition from indirect-to-direct band gap as well as a reduction in the number of layers of the WS_2 nanoflowers. The formation of WS_2 was confirmed by XPS and XRD with traces of the oxide phase, WO_3. XPS analysis also confirmed the successful capping of the nanoflowers. The WS_2 nanoflowers exhibited a good response and selectivity for ammonia.

Keywords: colloidal synthesis; hierarchical; nanoflowers; ammonia; gas sensing properties

1. Introduction

Effective air quality management requires regular monitoring of both indoor and outdoor environments for the detection of harmful and toxic pollutants such as NH_3. Even though semiconducting metal oxides (SMOs) are still the front runners in the category of chemiresistive gas sensors, their high energy input requirement (300–500 °C) is a major drawback [1,2]. Therefore, an alternative that can be incorporated into low-power operating air monitoring systems and still provide a high response even at room temperature (RT) is sought [3]. As a result, the gas sensing research community is putting a lot of effort into the research on other materials such as the transition metal dichalcogenides (TMDCs). TMDCs are layered semiconducting materials with outstanding electronic, chemical and mechanical stabilities [3,4] and a large surface-to-volume ratio [3,5]. Another interesting feature about TMDCs is their layer-dependent properties such as the band gap [4], indirect-to-direct band gap transition [6,7], electronic transport [5,8] and gas sensing [5]. WS_2 is steadily catching up with its TMDC family member, MoS_2, with respect to the research dedicated to its potential to detect NH_3. Huo et al. reported on the dynamic response of exfoliated multilayer WS_2 nanoflakes upon exposure to the reducing gas NH_3 at room temperature [9]. A transfer of charge between the adsorbed NH_3 and the exfoliated multilayer WS_2 nanoflakes resulted in increased conductivity. NH_3 donated electrons to the WS_2

nanoflakes, thereby inducing an n-type behavior. High NH_3 room temperature sensitivity was also observed with thin films of WS_2 obtained via a plasma-assisted synthesis [6]. However, the thin films displayed incomplete recovery. This is a common feature with nanomaterial-based sensors operating at low temperatures; the thin films can be subjected to annealing or UV light illumination to speed up the recovery. Remarkable selectivity to interferents, good selectivity, significant response/recovery rates and a p-type response was reported by Li and co-workers when WS_2 nanoflakes produced by ball milling commercial powders were exposed to NH_3 at 20–200 °C [10]. The sensor response increased with an increase in humidity level (up to 73% relative humidity, RH).

The influence of layer numbers on the recovery rate after removal of NH_3 gas also came under scrutiny in Qin et al.'s study [11]. The WS_2 thin films in this study were fabricated from nanosheets which were obtained via lithium ion intercalation. The monolayer-based thin film had the shortest recovery time compared to its few-layered and bulk counterparts. It was proposed that the NH_3 that is in the interlayers of WS_2 is not easily desorbed, hence the slow or incomplete recovery by few-layered thin films. Results from a study by Perozzi and co-workers on the thermal stability of thin films prepared from commercially bought WS_2 revealed progressive oxidation to WO_3 within the 25–450 °C range [12]. Changes in morphology were noted at 150–250 °C and regarded as the indication of the formed WS_2/WO_3 composite. The gas sensing performance of the WS_2/WO_3 composite towards NH_3 decreased at annealing temperatures above 150 °C. Meanwhile, the 150 °C annealed composite recovered completely and displayed no cross sensitivity to water vapor at 60% RH. High sensitivity and fast recovery to room temperature NH_3 sensing and p-type character were shown by the hydrothermally prepared nanocomposite of Pt QDs/WS_2 nanosheets [13]. Other composites, such as nanosheets of WS_2 | O [3] and WS_2/TiO_2 [14], also exhibited high sensitivity, excellent selectivity and fast recovery at room temperature.

The nanoflower morphology presents a larger surface area, a larger number of active sites at the edges of the WS_2 layers and many interlayer spaces, which are all desirable in gas sensing. To exploit the properties of WS_2 nanomaterials, methods that enable precise control of the morphology are required. The reported synthetic routes for WS_2 nanoflowers are hydrothermal [15–23] and CVD [24,25]. Colloidal synthesis also offers precise control of the reaction parameters in order to obtain desirable morphology. It is catalyst-free, template-free, one-pot, easily scalable and short one-step synthesis at relatively low temperatures. It also accommodates the use of a capping agent which offers protection of the nanoparticles against agglomeration [26], modifies the surface of the nanoparticles, may introduce new functionalities [27] and can influence the type of morphology formed [28]. Oleylamine (OLA), an N-terminated ligand, is suitable for transition metal semiconductors. OLA is low cost, and can act as a solvent and reducing agent, thereby eliminating the use of many chemicals; it can also lower the decomposition temperature of a metal precursor. Nanoparticles capped by OLA are easily dispersed in various organic solvents with improved properties and potential applications in various fields [26,29]. Colloidally synthesized WS_2 nanoflowers have not been extensively reported and their gas sensing potential has not been explored.

In this study, a colloidal method with OLA as both solvent and capping agent was followed to obtain hierarchical WS_2 nanoflowers. The nanoflowers were obtained after 45 min and were tested at room temperature for potential ammonia gas sensing properties. A good response and higher selectivity were observed towards ammonia vapors than with acetone, chloroform, ethanol and toluene. The dependence of sensing properties of a particular sensor on its method of synthesis is well known. To our knowledge, colloidal hierarchical nanoflowers of WS_2 have not been synthesized for application in gas sensing.

2. Materials and Methods

2.1. Chemicals

Analytical grade tungstic acid (H_2WO_4), thiourea ($CS(NH_2)_2$), oleylamine (OLA), ammonium hydroxide (NH_4OH), ethanol (CH_3CH_2OH), hexane (C_6H_{14}), chloroform

($CHCl_3$), toluene ($C_6H_5CH_3$), acetone ($(CH_3)_2CO$) and isopropyl alcohol (C_3H_8O) were purchased from Sigma-Aldrich, Johannesburg, South Africa and DieLab, Curitiba, Brazil. Interdigitated electrodes (IDEs) of electroless nickel immersion gold (ENIG) (18 pairs, 7.9 mm long and 0.1 mm apart) were purchased from Micropress SA, Curitiba, Brazil.

2.2. Synthesis of WS_2 Nanoflowers

Hierarchical nanoflowers of WS_2 were synthesized by mixing H_2WO_4 (0.05 mol) and $CS(NH_2)_2$ (0.2 mol) in 20 mL of degassed OLA. The mixture was heated at 25 °C with continuous stirring under N_2 gas flow for 15 min in a three-neck round-bottom flask. The temperature was increased rapidly to 320 °C to allow for the decomposition of both precursors and held at this temperature for 45 min. After cooling the black reaction mixture for 5 min, ethanol was added in order to separate the colloids. WS_2 nanoflowers were collected by centrifugation and washed several times with a mixture of ethanol and hexane (1:1). The WS_2 black powders were dried at room temperature.

2.3. Material Characterization

2.3.1. Optical Characterization

The WS_2 powder was dispersed in $CHCl_3$ and placed in quartz cuvettes (1 cm path length) for UV–Vis absorption and PL spectral measurements on the Specord 50 Analytik Jena UV–Vis spectrophotometer and Agilent Cary Eclipse fluorescence spectrometer, respectively. Raman spectroscopy (Bruker Senterra Infinity 1 software, 50× optical objective, 532 nm laser wavelength, 0.2 mV laser power and integration power of 15 s) measurements of the dry powder of WS_2 nanoflowers were used to estimate the number of layers.

2.3.2. Structural Characterization

Measurements were performed on the WS_2 powder with the Bruker MeasSrv (D2-205530)/D2-205530 diffractometer to shed light on the structure and phase of the powdered nanoflowers. X-ray photoelectron spectroscopy measurements were carried out with a PHI 5000 Versaprobe—Scanning ESCA Microprobe (100 µm 25 W 15 kV Al monochromatic X-ray beam) to determine the surface properties of the powders. Sizes and morphologies of the nanomaterials were studied using an FEI Nova NanoLab FIB/SEM and a JEOL JEM-2100 field emission gun transmission electron microscope (200 kV) Chemical composition of the crystal structure was analyzed with energy-dispersive X-ray spectroscopy (EDS) integrated into the TEM instrument.

2.4. Device Fabrication and Gas Sensing Measurements

The WS_2 nanoflower-based sensor was fabricated by drop casting 20 µL of the 5 mg/mL WS_2 toluene dispersion on clean IDEs. The sensor was dried in an oven at 130 °C for 30 min. A surface profiler (Dektak XT; Bruker) was used to measure the thickness of the film (about 600 nm). A custom-made gas chamber, depicted in Figure 1, housed the sensor. The gas chamber was grounded and stabilized for 1 h before measurements were started.

An LCR meter (Agilent 4284A 20 Hz–1 MHz Precision LCR meter) was attached to a computer interfaced with a GPIB for data acquisition and set at an operational voltage and frequency of 1000 mV and 10 kHz, respectively. A large variation in conductance and relative signal-to-noise were obtained at these parameters. The measurements were performed in the dark and under dry nitrogen to provide a controlled atmosphere. The sensor was exposed to incremental concentrations of NH_3 (NH_4OH was used as the source of NH_3) at RT (~23 °C) and 25% RH. A 50 s stabilizing period followed by introduction of 1.5 µL of NH_4OH (analyte) at every 200 s was applied per measurement. The time interval was enough to evaporate the analyte and saturate the chamber. The measurements were taken with concentrations of NH_4OH in the range of 240–958 ppm. The selective character of the sensor was established by exposing it to incremental concentrations of interferents such as acetone, chloroform, ethanol and toluene. Response and recovery

measurements were carried out to determine how fast the sensor responds to NH_3 and how fast it recovers to its initial chemical status after NH_3 is removed. The effect of humidity on the sensor's gas performance was determined by measuring its response to NH_3 under various RH levels.

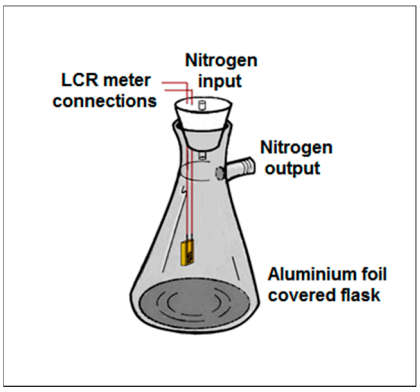

Figure 1. Schematic representation of the gas chamber used for sensor measurements.

3. Results

3.1. Characterization of WS_2 Nanoflowers

The crystal phase, crystallinity and composition of the WS_2 nanoflowers were determined with PXRD. The diffraction patterns, as shown in Figure 2, confirmed the nanoflowers to be the 2H-WS_2 polytype according to PDF No: 00-002-0131\JCP2.2CA. The diffraction peaks correspond to the (002), (004), (101), (103), (006), (008) and (200) planes. The prominence of the (002) plane suggested the existence of more than one layer of WS_2 with good crystallinity while its broadness is an indication of a reduction in size. Closer analysis hinted at partial oxidation based on the small peak at 29.5° (denoted by an asterisk) which was assigned to WO_3. This came as no surprise as WS_2 is known for spontaneous oxidation.

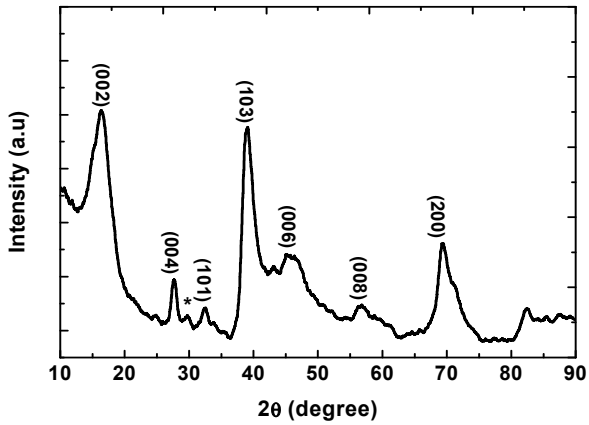

Figure 2. X-ray diffraction pattern of WS_2 nanoflowers. The peak at 29.5° (denoted by *) was assigned to WO_3.

XPS studies provided detailed composition of the nanoflowers. The W and S peaks are clearly displayed on the survey spectrum, shown in Figure 3. Partial oxidation of WS_2 to WO_3 was confirmed by the presence of the O 1s peak. The oxygen peak is also attributed to the oxidation of OLA. The successful capping of the nanoflowers by the organic ligand OLA was confirmed by the presence of the strong C 1s peak. Atewolegun et al. used XPS in their studies to confirm the success of ligand exchange on colloidal quantum dots [30]. The capping of the samples is further confirmed by the large carbon composition (77.4%) of the sample, as seen in Table 1.

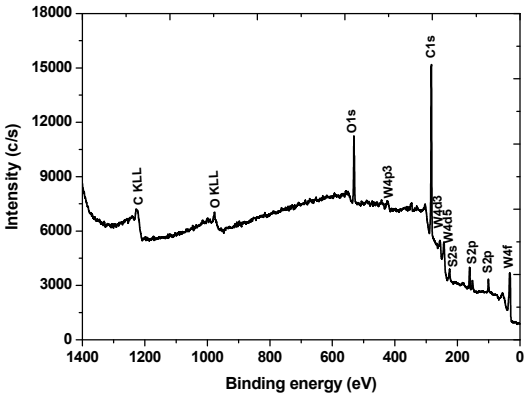

Figure 3. XPS survey spectrum of WS_2 nanoflowers.

Table 1. Summary of the atomic composition stoichiometric assignments obtained from the fitting of the XPS spectra of WS_2 nanoflowers.

Element	Atomic %	Peak Binding Energy (eV)	Assignments	Peak Area %
C	77.4	284.8	C-C	91
		286.3	C-O	6
		288.9	O-C=O	3
O	10.8	532.2	C-O	100
W	3.7	30.9	WS_2	41
		33.2	WS_2	38
		34.4	W^{5+}	6
		36.3	WO_3	15
S	6.2	160.5	S_2W def.	9
		161.6	S_2W	60
		162.8	S_2W	31

Figure 4 shows the high-resolution core level spectra of WS_2 with the deconvoluted C-C peak by OLA. The O 1s, C-O and O-C=O peaks were attributed to the oxidation of OLA. Four components of the W4f core level spectrum were identified; W $4f_{7/2}$ (30.9 eV), W $4f_{5/2}$ (33.2 eV) doublet, W $5p_{3/2}$ (34.4 eV) and WO_3 (36.3 eV). Meanwhile, the W $4f_{7/2}$ and W $4f_{5/2}$ are ascribed to the 2H-WS_2 polytype. W $5p_{3/2}$ is attributed to the partially coordinated W in WO_3. The S2p spectrum has three peaks, S_2Wdef (160.5 eV), S_2W (161.6 eV) and S_2W (162.8 eV) which were observed in the deconvoluted core level spectrum.

Raman spectroscopy was used to estimate the number of the layers in the nanoflowers. The WS_2 nanoflowers showed Raman features which are characteristic of the second order longitudinal acoustic 2LA(M) and out-of-plane $A_{1g}(\Gamma)$ at approximately 351 cm^{-1} and 417 cm^{-1}, respectively, as seen in Figure 5. The shoulder peak at 313 cm^{-1} belongs to the in-plane $E_{12g}(\Gamma)$. The shift to lower frequencies from bulk for both $A_{1g}(\Gamma)$ and 2LA(M) (356 and 421 cm^{-1}, respectively) is associated with decreasing interlayer interactions by van der Waals forces. This suggested the formation of few layers, in agreement with Varghese et al. [31] and Tan et al. [32]. The calculated frequency difference between $A_{1g}(\Gamma)$ and 2LA(M) as well as the intensity of 2LA(M), suggesting a reduction in size from bulk to a few layers.

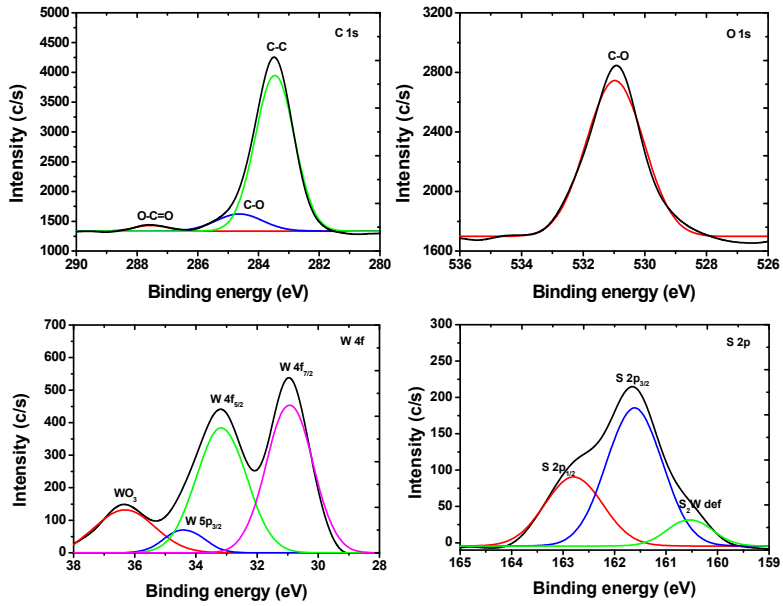

Figure 4. High-resolution core level spectra of WS_2 nanoflowers with focus on C1s, O1s, W4f and S2p. The blue, green, red and purple lines are their respective deconvoluted spectra.

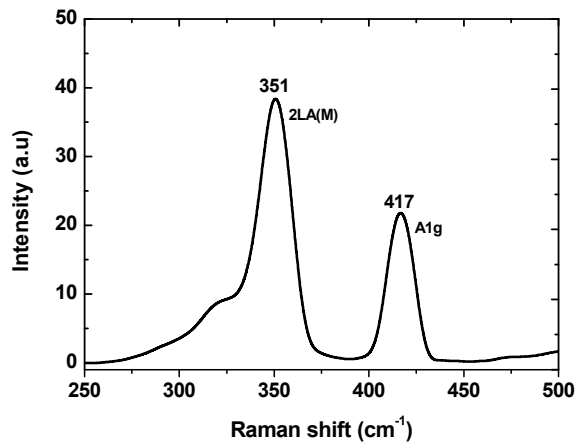

Figure 5. Raman spectra of WS_2 nanoflowers.

SEM analysis of as-synthesized WS_2 revealed nanosheets arranged as petals to form the nanoflower morphology, as seen from Figure 6A,B. These nanoflowers self-assembled to form hierarchical structures. Figure 6B gives a clearer picture of the well-ordered nanosheets with interspaces. This feature of nanoflowers translates to a larger surface area, which is ideal for gas sensing.

Meanwhile, the TEM image from Figure 7A confirmed that the nanoflowers were made up of individual nanosheets. The edges of the nanosheets are exposed and serve as active sites. The microspheres in Figure 7B are consistent with the nanoflower morphology recorded by SEM in Figure 6A,B.

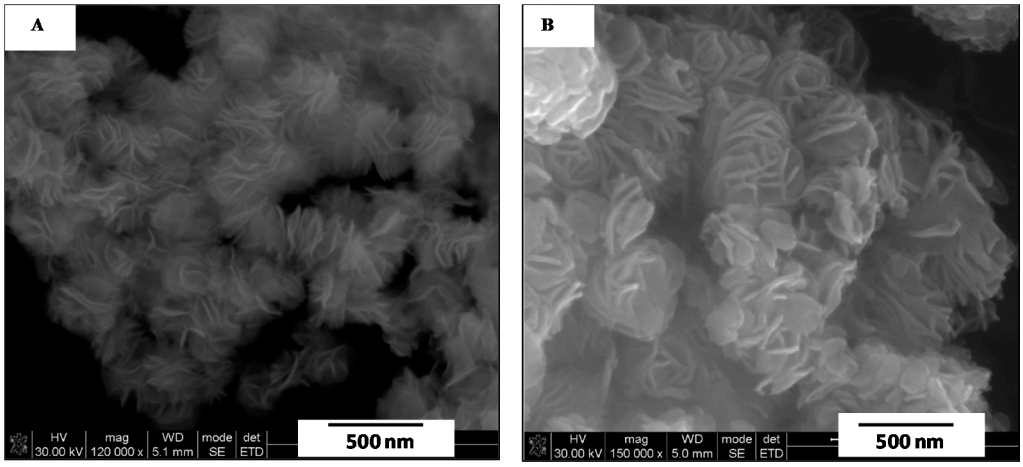

Figure 6. (**A**,**B**) SEM characterization of WS_2 nanoflowers.

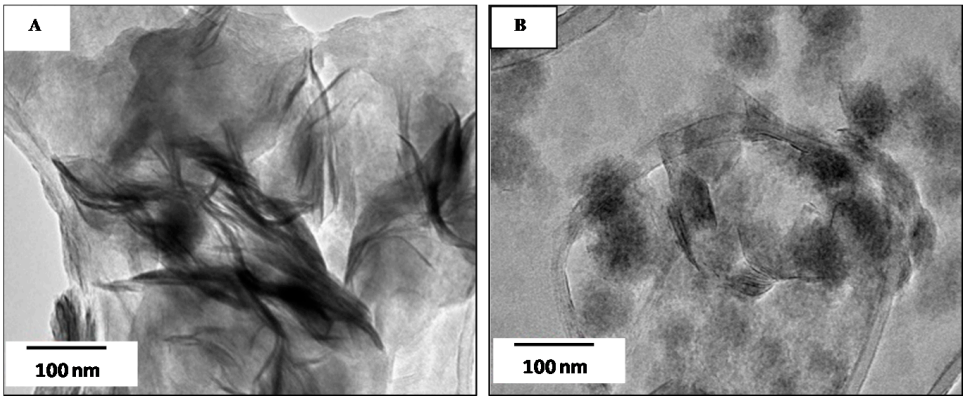

Figure 7. (**A**,**B**) TEM images of WS_2 nanoflowers.

UV–Vis absorption and photoluminescence spectroscopy further confirmed the reduced size of WS_2. Figure 8 shows the blue-shifted 625–630 nm and 505–515 nm peaks corresponding to the excitons A and B (636 and 525 nm for bulk WS_2, respectively) [33]. The existence of few layers was further suggested by the diminished photoluminescence peak, shown in Figure 8. A similar result was reported by Gutiérrez et al. and was said to be the result of a competition between indirect and direct transitions [34].

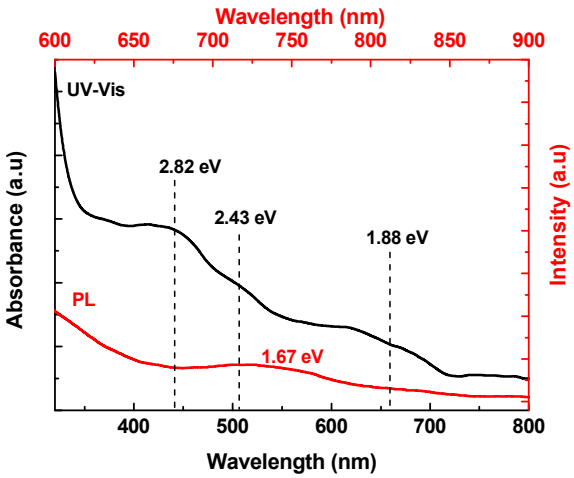

Figure 8. UV–Vis absorption (black line) and photoluminescence spectra (red line) of WS_2 nanoflowers.

3.2. Gas Sensing Properties of the WS_2 Nanoflowers

The sensing principle of thin films of semiconducting TMDCs is generally based on the change in conductance due to the reaction of the gas that is adsorbed on the surface. An electric charge is transferred between the gas (target analyte) and the active material (WS_2 nanoflowers), causing changes in the electrical properties of the sensing material. Preliminary gas sensing measurements at RT under dry N_2 (25% RH) revealed a fast decrease in the conductance, G, of the WS_2 nanoflowers. The sharp decrease in conductance, G, as shown in Figure 9A (red curve), was due to the adsorption of NH_3 gas molecules on the surface of the WS_2 nanoflowers. The negative slope (sensitivity = -7.99 ppm^{-1}) as shown in Figure 9B confirmed the decrease in conductance. The response was linearly proportional to the concentration of NH_3. NH_3 is a Lewis base and therefore serves as an electron donor. In this work, the NH_3 lone pair electron was transferred to the conduction band of the WS_2 nanoflower-based sensor upon adsorption. The reduction in the electrical conductance suggested that positive holes are the main charge carriers on the surface of WS_2 nanoflowers, hence the p-type doping behavior. This is due to the depletion of positive (hole) charge carriers on the sensor surface by the negative charge carriers from NH_3. A similar p-type behavior was observed previously for MoS_2 and WS_2 sensors by Järvinen et al. [35]. The gas response of the WS_2 nanoflower-based sensor to NH_3 vapors was determined from the variation in the conductance, G, by using $\Delta G/G_0$ in the equation below:

$$S = \frac{\Delta G}{G_0} \tag{1}$$

where $\Delta G = (G - G_0)$. G is the maximum conductance under NH_3 vapors while G_0 is conductance under dry N_2. The sensitivity, S (in ppm^{-1}), of the sensor was determined from the slope of the fit.

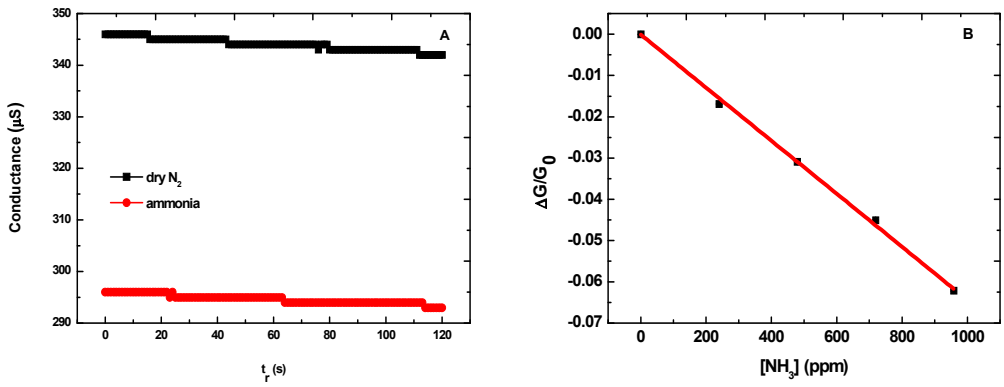

Figure 9. Response of the WS_2 nanoflower-based sensor at RT. (**A**) Conductance under dry N_2 conditions (black curve) and after exposure to 958 ppm of NH_3 (red curve) as a function of time. (**B**) Sensitivity of the WS_2 nanoflowers to NH_3 concentrations ranging from 240 to 958 ppm. Relative variation in the conductance to NH_3 concentrations ranging from 240 to 958 ppm. The solid red line represents the linear fit to the experimental data (black squares). The slope of the fit is the sensitivity of the WS_2 nanoflower-based sensor.

Specificity or selectivity is another parameter that determines the practical use of a sensor. It is the ability of a sensor to detect the target analyte in the presence of other contaminants. The specificity value for a sensor is between 0 and 1 with a value closer to 1 representing high selectivity of the sensor for the target analyte relative to the interferents. Consider a particular sensor and a set of n species; the specificity to the particular species i, δ_i can defined as follows:

$$\delta_i = \frac{\left(\Delta G/G_0\right)_i}{\sum_{j=1}^{n}\left(\Delta G/G_0\right)_j} \tag{2}$$

The equation above was adapted from Llobet et al. [36] and was used to calculate the specificity value (δ) of the sensor to NH_3 and the interferents. In this work, the sensor showed higher selectivity for ammonia than to acetone, chloroform, ethanol and toluene, as shown in Figure 10. The specificity values of the vapors are summarized in Table 2. Therefore, WS_2 nanoflowers have the potential for use as elements in chemical sensor arrays.

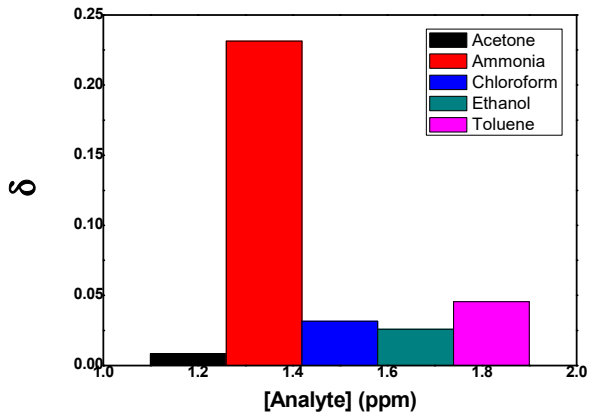

Figure 10. Response of the WS_2 nanoflowers to 1.5 µL of each analyte at 25% RH.

Table 2. Specificity values of the sensor to each chemical vapor.

Analyte	Concentration (ppm)	Specificity
Acetone	502	0.086
Ammonia	240	0.23
Chloroform	444	0.031
Ethanol	632	0.026
Toluene	352	0.045

For practical purposes, a sensor must respond fast upon exposure to the target gas and recover just as fast when the gas is removed. The characteristic sensor curve (dynamic range) shown in Figure 11 was analyzed and used to estimate the response and recovery speed at incremental concentrations of NH_3. The conductance of the sensor decreased sharply (~28 s) upon exposure to NH_3, giving a negative response, and slowly recovered (~42 s) when removed from NH_3. Slow recovery at RT is common to TMDC thin film-based NH_3 sensors [11,37] due to strong interactions between NH_3 molecules and the active layer. This leads to analyte accumulation on the surface of the sensor [38].

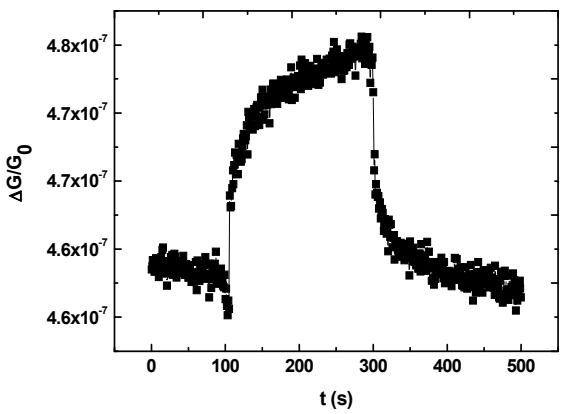

Figure 11. Response and recovery curve for WS_2 sensor to 240 ppm of NH_3 in ambient atmosphere.

Theoretical calculations predicted that the analyte is physically adsorbed on the surface of a perfect 2D monolayer [39]. However, this is not the case for few-layered and bulk WS_2 sensors where the NH_3 molecule can be inserted into the inner layers and interact with the two adjacent layers, as shown in Figure 12 below [11].

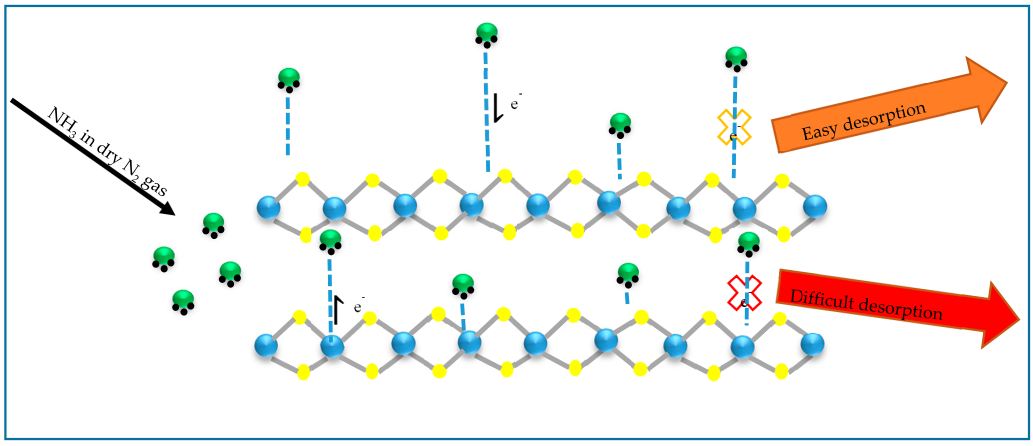

Figure 12. Schematic illustration of the interfacial interaction of NH_3 molecules with the surface and interlayer of WS_2. The illustration is adapted from Qin, et al. [11].

Intercalation compounds such as $(NH4^+)_X(NH_3)_Y(WS_2)^{X-}$ may be formed. The intercalated NH_3 molecules are more difficult to desorb than the surface molecules. This behavior is similar to the intercalation and deintercalation processes of NH_3 with layered TiS_2 and TaS_2 which were detailed by McKelvy and Glaunsinger [40]. Based on the confirmation of the existence of a few layers of WS_2 by XRD, Raman and TEM, the argument of intercalated NH_3 molecules can be applied in this study to explain the slow recovery of the sensor. Furthermore, the nanoflower morphology has interspaces which provide more reactive sites; thus, more NH_3 molecules end up deeper inside the layers, leading to a slow recovery. It is worth mentioning that defects are introduced during colloidal synthesis, and this too provides more reactive sites than the perfect lattice of a 2D monolayer. The WS_2 nanoflower-based sensor recovered completely after irradiation with UV light for 60 min or heating in an oven for 10 min at 100 °C.

Water molecules are easily adsorbed on the surface of the sensor, leading to an increase or decrease in its performance. This is common with RT chemical sensors. As the WS_2 nanoflower-based sensor is designed for application in RT sensing of NH_3, it was imperative to measure its performance under various levels of humidity. Figure 13 illustrates the response of the sensor at different RH conditions. The effect of humidity on the gas sensing performance of WS_2 nanoflowers was found to be more pronounced at 97% RH.

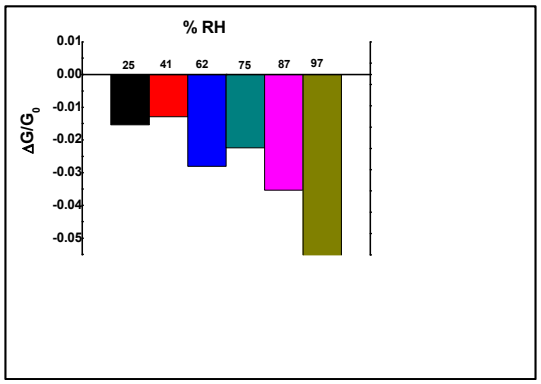

Figure 13. Response of the WS_2 sensor towards 240 ppm of NH_3 at room temperature under various humidity conditions (25, 41, 62, 75, 87 and 97%).

The increase in NH_3 response in the presence of humidity could be attributed to the increased acidity due to the water molecules on the surface of the WS_2 nanoflower-based sensor [10]. Such an increase can be explained by the hydroxylation reaction below:

$$SO_4^{2-}\ (WS_2\ \text{surface}) + H_2O \leftrightarrow H^+ + SO_4^{2-} + OH^- \quad (3)$$

The NH_3 molecules donated more electrons to the already acidic surface of the WS_2 sensor, resulting in the observed increase in response.

4. Conclusions

WS_2 nanoflowers were successfully synthesized after 45 min via a simple colloidal route. The colloidal nanoflowers displayed a good response and higher selectivity towards NH_3 vapors relative to acetone, ethanol, toluene and chloroform. The gas sensing performance exhibited by the nanoflowers is evidence that the partial oxidation did not adversely compromise it. Humidity interference was established and its significance was observed at very high % RH values. Evidence of incomplete recovery due to the strong interaction between NH_3 molecules and the sensor was observed. The sensor has potential for use as an active material in RT chemiresistive sensors and sensor arrays. Studies are underway to develop strategies to improve the overall gas sensing performance of the WS_2 nanoflowers by doping with metal oxides, metals, carbon materials, perovskites and other TMDCs. The focus is on reducing the recovery time, enhancing the sensitivity and selectivity to NH_3 and slowing down oxidation. The sensor will also be tested for sensitivity to NO_2 and CO.

Author Contributions: S.S.G., N.M., R.R. and I.A.H. conceptualized the experiments. S.S.G., S.L.M., Z.N., P.O.F. and R.R. performed the experiments. S.S.G. and R.R. analyzed the data. S.S.G. and R.R. prepared the original draft. The review and editing of the manuscript were done by S.S.G., R.R., M.A., I.A.H., N.M., E.C.L., M.J.M., N.M. and I.A.H. supervised the research project. All authors have read and agreed to the published version of the manuscript.

Funding: This research was funded by the National Research Foundation (TTK180419322895), the University of the Witwatersrand and the Department of Higher Education.

Institutional Review Board Statement: Not applicable.

Informed Consent Statement: Not applicable.

Data Availability Statement: Not applicable.

Acknowledgments: The authors acknowledge the Department of Physics, Universidade Federal do Paranà, Brazil for technical support and materials used for experiments.

Conflicts of Interest: The authors declare no conflict of interest.

References

1. Ko, K.Y.; Park, K.; Lee, S.; Kim, Y.; Woo, W.J.; Kim, D.; Song, J.-G.; Park, J.; Kim, H. Recovery Improvement for Large-Area Tungsten Diselenide Gas Sensors. *ACS Appl. Mater. Interfaces* **2018**, *10*, 23910–23917. [CrossRef]
2. Kaewmaraya, T.; Ngamwongwan, L.; Moontragoon, P.; Jarernboon, W.; Singhd, D.; Ahujad, R.; Karton, A.; Hussain, T. Novel green phosphorene as a superior chemical gas sensing material. *J. Hazard. Mater.* **2021**, *401*, 123340. [CrossRef] [PubMed]
3. Zheng, Y.; Sun, L.; Liu, W.; Wang, C.; Dai, Z.; Ma, F. Tungsten oxysulfide nanosheets for highly sensitive and selective NH_3 sensing. *J. Mater. Chem. C* **2020**, *8*, 4206–4214. [CrossRef]
4. Kumar, R.; Goel, N.; Hojamberdiev, M.; Kumar, M. Transition metal dichalcogenides-based flexible gas sensors. *Sens. Actuators A* **2020**, *303*, 111875. [CrossRef]
5. Wang, W.; Cao, J.; Zhou, J.; Chen, J.; Liu, J.; Deng, H.; Zhang, Y.; Li, X. Highly enhanced performance for sensing by monolayer 1T′ WS_2 with atomic vacancy. *Microelectron. Eng.* **2020**, *223*, 111215. [CrossRef]
6. Gatensby, R.; McEvoy, N.; Lee, K.; Hallam, T.; Berner, N.C.; Rezvani, E.; Winters, S.; O'Brien, M.; Duesberg, G.S. Controlled synthesis of transition metal dichalcogenide thin films for electronic applications. *Appl. Surf. Sci.* **2014**, *297*, 139–146. [CrossRef]
7. Samadi, M.; Sarikhani, N.; Zirak, M.; Zhang, H.; Zhang, H.-L.; Moshfegh, A.Z. Group 6 transition metal dichalcogenide nanomaterials: Synthesis, applications and future perspectives. *Nanoscale Horiz.* **2018**, *3*, 90–204.
8. Pumera, M.; Loo, A.H. Layered transition-metal dichalcogenides (MoS_2 and WS_2) for sensing and biosensing. *Trends Anal. Chem.* **2014**, *61*, 49–53. [CrossRef]

9. Huo, N.; Yang, S.; Wei, Z.; Li, S.-S.; Xia, J.-B.; Li, J. Photoresponsive and Gas Sensing Field-Effect Transistors based on Multilayer WS_2 Nanoflakes. *Sci. Rep.* **2014**, *4*, 5209. [CrossRef]
10. Li, X.; Li, X.; Li, X.; Wang, J.; Zhang, Z. WS_2 Nanoflakes Based Selective Ammonia Sensors at Room Temperature. *Sens. Actuators B Chem.* **2017**, *240*, 273–277. [CrossRef]
11. Qin, Z.; Zeng, D.; Zhang, J.; Wu, C.; Wen, Y.; Shan, B.; Xie, C. Effect of layer number on recovery rate of WS_2 nanosheets for ammonia detection at room temperature. *Appl. Surf. Sci.* **2017**, *414*, 244–250. [CrossRef]
12. Perrozzi, F.; Emamjomeh, S.M.; Paolucci, V.; Taglier, G.; Ottaviano, L.; Cantalini, C. Thermal Stability of WS_2 Flakes and Gas Sensing Properties of WS_2/WO_3 Composite to H_2, NH_3 and NO_2. *Sens. Actuators B Chem.* **2017**, *243*, 812–822. [CrossRef]
13. Ouyang, C.; Chen, Y.; Qin, Z.; Zeng, D.; Zhang, J.; Wang, H.; Xi, C. Two-dimensional WS_2-based nanosheets modified by Pt quantum dots for enhanced room-temperature NH_3 sensing properties. *Appl. Surf. Sci.* **2018**, *455*, 45–52. [CrossRef]
14. Qin, Z.; Ouyang, C.; Zhang, J.; Wan, L.; Wang, S.; Xie, C.; Zeng, D. 2D WS_2 nanosheets with TiO_2 quantum dots decoration for high-performance ammonia gas sensing at room temperature. *Sens. Actuators B* **2017**, *253*, 1034–1042. [CrossRef]
15. Wu, Y.-C.; Liu, Z.-M.; Chen, J.-T.; Cai, X.-J.; Na, P. Hydrothermal fabrication of hyacinth flower-like WS_2 nanorods and their photocatalytic properties. *Mater. Lett.* **2017**, *189*, 282–285. [CrossRef]
16. Li, X.; Zhang, J.; Liu, Z.; Fu, C.; Niu, C. WS_2 nanoflowers on carbon nanotube vines with enhanced electrochemical performances for lithium and sodium-ion batteries. *J. Alloys Compd.* **2018**, *766*, 656–662. [CrossRef]
17. Nguyen, T.P.; Kim, S.Y.; Lee, T.H.; Jang, H.W.; Led, Q.V.; Kim, I.T. Facile synthesis of $W_2C@WS_2$ alloy nanoflowers and their hydrogen generation performance. *Appl. Surf. Sci.* **2020**, *504*, 144389. [CrossRef]
18. Srinivaas, M.; Wu, C.-Y.; Duh, J.-G.; Wu, J.M. Highly Rich 1T Metallic Phase of Few-Layered WS_2 Nanoflowers for Enhanced Storage of Lithium-Ion Batteries. *ACS Sustain. Chem. Eng.* **2019**, *7*, 10363–10370. [CrossRef]
19. Tekalgne, M.; Hasani, A.; Le, Q.V.; Nguyen, T.P.; Choi, K.S.; Lee, T.H.; Jang, H.W.; Luo, Z.; Kim, S.Y. CdSe Quantum Dots Doped WS_2 Nanoflowers for Enhanced Solar Hydrogen Production. *Phys. Status Solidi A* **2019**, *216*, 180085. [CrossRef]
20. Hasani, A.; Nguyen, T.P.; Tekalgne, M.; Le, Q.V.; Choi, K.S.; Lee, T.H.; Park, T.J.; Jang, H.W.; Kim, S.Y. The role of metal dopants in WS_2 nanoflowers in enhancing the hydrogen evolution reaction. *Appl. Catal. A Gen.* **2018**, *567*, 73–79. [CrossRef]
21. Cao, C.Z.; Peng, L.; Han, T. Synthesis of uniform WS_2 nanoflowers via a sodium silicate-assisted hydrothermal process. *J. Mater. Sci. Mater. Electron.* **2016**, *27*, 3821–3825. [CrossRef]
22. Liu, S.; Shen, B.; Niu, Y.; Xu, M. Fabrication of WS_2-nanoflowers@rGO composite as an anode material for enhanced electrode performance in lithium-ion batteries. *J. Colloid Interface Sci.* **2017**, *488*, 20–25. [CrossRef]
23. Cao, S.; Liu, T.; Zeng, W.; Hussain, S.; Peng, X.; Pan, F. Synthesis and characterization of flower-like WS_2 nanospheres via a facile hydrothermal route. *J. Mater. Sci. Mater. Electron.* **2014**, *25*, 4300–4305. [CrossRef]
24. Prabakaran, A.; Dillon, F.; Melbourne, J.; Jones, L.; Nicholls, R.J.; Holdway, P.; Britton, J.; Koos, A.A.; Crossley, A.; Nellist, P.D.; et al. WS_2 2D nanosheets in 3D nanoflowers. *Chem. Commun.* **2014**, *50*, 12360–12362. [CrossRef] [PubMed]
25. Zhang, X.; Wang, J.; Xu, H.; Tan, H.; Ye, X. Preparation and Tribological Properties of WS_2 Hexagonal Nanoplates and Nanoflowers. *Nanomaterials* **2019**, *9*, 840. [CrossRef] [PubMed]
26. Javed, R.; Zia, M.; Naz, S.; Aisida, S.O.; Ain, N.u.; Ao, Q. Role of capping agents in the application of nanoparticles in biomedicine and environmental remediation: Recent trends and future prospects. *J. Nanobiotechnol.* **2020**, *18*, 172. [CrossRef]
27. Campisi, S.; Schiavoni, M.; Chan-Thaw, C.E.; Villa, A. Untangling the Role of the Capping Agent in Nanocatalysis: Recent Advances and Perspectives. *Catalysts* **2016**, *6*, 185. [CrossRef]
28. Phan, C.H.; Nguyen, H.M. Role of Capping Agent in Wet Synthesis of Nanoparticles. *J. Phys. Chem. A* **2017**, *121*, 3213–3219. [CrossRef]
29. Gulati, S.; Sachdeva, M.; Bhasin, K.K. Capping Agents in Nanoparticle Synthesis: Surfactant and Solvent System. *AIP Conf. Proc.* **2018**, *1953*, 030214.
30. Atewologun, A.; Ge, W.; Stiff-Roberts, A.D. Characterization of Colloidal Quantum Dot Ligand Exchange by X-ray Photoelectron Spectroscopy. *J. Electron. Mater.* **2013**, *42*, 809–814. [CrossRef]
31. Wang, X.; Gu, D.; Li, X.; Lin, S.; Zhao, S.; Rumyantseva, M.N.; Gaskov, A.M. Reduced Graphene Oxide Hybridized with WS_2 Nanoflakes based Heterojunctions for Selective Ammonia Sensors at Room Temperature. *Sens. Actuators B Chem.* **2019**, *282*, 290–299. [CrossRef]
32. Lee, J.-H. Gas Sensors Using Hierarchical and Hollow Oxide Nanostructures: Overview. *Sens. Actuators B Chem.* **2009**, *140*, 319–336. [CrossRef]
33. Li, Y.-X.; Guo, Z.; Su, Y.; Jin, X.-B.; Tang, X.-H.; Huang, J.-R.; Huang, X.-J.; Li, M.-Q.; Liu, J.-H. Hierarchical Morphology-Dependent Gas-Sensing Performances of Three-Dimensional SnO_2 Nanostructures. *ACS Sens.* **2017**, *2*, 102–110. [CrossRef]
34. Gutiérrez, H.R.; Perea-López, N.; Elías, A.L.; Berkdemir, A.; Wang, B.; Lv, R.; López-Urías, F.; Crespi, V.H.; Terrones, H.; Terrones, M. Extraordinary Room-Temperature Photoluminescence in Triangular WS_2 Monolayers. *Nano Lett.* **2013**, *13*, 3447–3454. [CrossRef]
35. Järvinen, T.; Lorite, G.S.; Peräntie, J.; Toth, G.; Saarakkala, S.; Virtanen, V.K.; Kordas, K. WS_2 and MoS_2 thin film gas sensors with high response to NH_3 in air at low temperature. *Nanotechnology* **2019**, *30*, 405501. [CrossRef]
36. Llobet, E.; Molas, G.; Molinàs, P.; Calderer, J.; Vilanova, X.; Brezmes, J.; Sueiras, J.E.; Correiga, X. Fabrication of Highly Selective Tungsten Oxide Ammonia Sensors. *J. Electrochem. Soc.* **2000**, *147*, 776–779. [CrossRef]

37. Late, D.J.; Huang, Y.-K.; Liu, B.; Acharya, J.; Shirodkar, S.N.; Luo, J.; Yan, A.; Charles, D.; Waghmare, U.V.; Dravid, V.P.; et al. Sensing behavior of atomically thin-layered MoS_2 transistors. *ACS Nano* **2013**, *7*, 4879–4891. [CrossRef]
38. Marr, I.; Groß, A.; Moos, R. Overview on Conductometric Solid-state Gas Dosimeters. *J. Sens. Sens. Syst.* **2014**, *3*, 29–46. [CrossRef]
39. Zeng, Y.; Lin, S.; Gu, D.; Li, X. Two-Dimensional Nanomaterials for Gas Sensing Applications: The Role of Theoretical Calculations. *Nanomaterials* **2018**, *8*, 851. [CrossRef]
40. McKelvey, M.J.; Glaunsinger, W.S. On the Intercalation and Deintercalation Mechanisms for Ammoniated Titanium Disulfide. *Solid State Ion.* **1987**, *25*, 287–294. [CrossRef]